Silver nanoparticles incorporated local montmorillonite clay modified carbon paste electrode for the voltammetric determination of Arsenic (III) in aqueous solution

Mekonnen Mihiret Dessie and Abebaw Adgo Tsegaye[*]

Department of Chemistry, Bahir Dar University, PO Box 79, Bahir Dar, Ethiopia

ABSTRACT

A sensitive electrochemical method was developed to determine arsenic (III) using silver nanoparticles incorporated local montmorillonite clay nanocomposites modified carbon paste electrode (Ag-NPs/MT/CPE) in aqueous solution. Electrochemical properties of carbon paste electrode (CPE) modified by Ag-NPs/MT nanocomposite were studied using cyclic voltammetry and electrochemical impedance spectroscopy in the presence of 10 mM $K_3Fe(CN)_6^{3-/4-}$/0.1 M KCl aqueous solution as well as in the presence of 100 µg/mL As (III) in 0.1 M PBS. Voltammograms acquired on Ag-NPs/MT/CPE showed an enhancement of the oxidation current density peak compared to the bare CPE. This is attributed mainly to the catalytic activity and improved surface to volume ratio of Ag-NPs/MT composite. The electrochemical sensor based on Ag-NPs/MT nanocomposite was constructed and used for the detection of As (III). Under optimized condition (pH 7, deposition potential-0.3 V and deposition time 60 s) the sensor exhibits sensitivity 0.02953µA/µg/mL and detection limit 38.2 µg/mL As (III). The Ag-NPs/MT/CPE has also shown good stability, it retained a response of 93.8% of the initial current after 12 days storage at room temperature. Therefore, the developed sensor can be a good candidate for electrochemical determination of As (III) in aqueous solution.

Key Words: Arsenic; Carbon paste electrode; Electrochemical sensor; Nanocomposite
DOI: https://dx.doi.org/10.4314/ejst.v16i3.2

INTRODUCTION

Heavy metals are defined as metallic elements that have a relatively high density compared to water. With the assumption that heaviness and toxicity are inter-related, heavy metals also include metalloids, such as arsenic, that are able to induce toxicity at low level of exposure (Duffus, 2002). In recent years, there has been an increasing ecological and global public health concern associated with environmental contamination by these metals. Also, human exposure has risen dramatically as a result of an exponential increase of their use in several industrial, agricultural, domestic and technological applications (Bradl, 2006). Sources of heavy metals in

---

[*] Corresponding author's email: abebawadgo@gmail.com

the environment include geogenic, industrial, agricultural, pharmaceutical, domestic effluents, and atmospheric sources (He *et al.*, 2005). Environmental pollution is very prominent in point source areas such as mining, smelters and other metal-based industrial operations. Environmental contamination can also occur through metal corrosion, atmospheric deposition, soil erosion of metal ions and leaching of heavy metals, sediment re-suspension and metal evaporation from water resources to soil and ground water (Haneef and Akıntuğ, 2016). In biological systems, heavy metals have been reported to affect cellular organelles and components such as cell membrane, mitochondrial, lysosome, endoplasmic reticulum, nuclei, and some enzymes involved in metabolism, detoxification, and damage repair. Metal ions have been found to interact with cell components such as DNA and nuclear proteins, causing DNA damage and conformational changes that may lead to cell cycle modulation, carcinogenesis or apoptosis (Beyersmann and Hartwig, 2008).

Arsenic, which is present in both organic and inorganic forms, causes adverse effect to human health because of its toxicity. Inorganic form of arsenic mainly exists in water in two forms, arsenate As (V) and arsenite (As (III)) ions. As (III) is more soluble in water and more toxic in comparison to As (V) (Luong *et al.*, 2014)). Even a very low concentration of arsenic present in water can cause skin diseases, cardiovascular diseases and cancer (Luong *et al.*, 2014). World Health Organization (WHO) recommends a maximum limit of arsenic in drinking water as 10 μg dm^{-3} (Martínez-Acuña *et al.*, 2016).

Several analytical methods have been exploited for the trace level determination of arsenic in various samples (Sitko *et al.*, 2015) such as x-ray fluorescence, inductively coupled plasma-atomic emission spectroscopy, atomic absorption spectrometry, graphite furnace atomic absorption spectrometry, etc. have been reported that are available and used for detecting, measuring, and monitoring the concentration of heavy metals in sewage water. Besides their valuable characteristics, these techniques suffer from some disadvantages such as heavy capital cost, expensive maintenance, need specialized technique, unsuitable for application in the field, insufficient sensitivity for very low concentrations of metals, analysis must be performed in a specialized laboratory by skilled person and tedious procedures are always required (Dharmalingam *et al.*, 2022). Thus, the development of other detection method that is sensitive, simple and rapid for determination of heavy metal levels is highly desirable for environmental monitoring and food safety applications. Electro analytical methods are advantageous over the other methods due to their fast, sensitive and selective determination (Das *et al.*, 2014).

Nowadays, considerable attention is devoted for the development of new nanostructured materials for the construction of electrochemical sensing platforms (Manivannan and Ramaraj, 2009). These new nanostructured materials can be

sourced from different constituents such as polymers (Rastogi *et al*., 2014), carbon-based materials (Davies *et al*., 2012), silica ((Manivannan and Ramaraj, 2009), clays (Premkumar and Ramaraj, 1997), etc. Among these materials, clays are widely used for the development of nanostructured materials because they are inexpensive, non-hazardous, easily available and very promising supports for the design and preparation of electrode material (Ramaraj, 2006). A large number of ion exchange sites available in clays are also beneficial for the incorporation of electro active species and nanoparticles (Das *et al*., 2014). Use of clays for the modification of electrode surfaces is already well established and clay-modified electrodes are constantly getting great interest for the construction of sensors and biosensors (Rossini *et al*., 2020). Therefore, in the present work, we synthesized a new nanostructured material based on local montmorillonite clay and Ag- NPs for the determination of As (III) in neutral condition.

MATERIALS AND METHODS

Chemicals and reagents

The following chemicals and reagents were utilized: distilled water, graphite powder (99.5%, Blulux, India), HNO_3 (69 %,) and KCl (99.5%) were purchased from Oxford Lab Chem. Mumbai, India, $AgNO_3$ (98%, Sigma Aldrich), sodium citrate (98% chemicals dyog, India), paraffin oil light, NaOH (98%), $K_3[FeCN_6]$ and HCl (37%) were obtained from Research lab fine chem. industry. India. Arsenic (III) standard (1000 ppm, CPI international, USA), K_2HPO_4 and KH_2PO_4 (98.5%, Research lab fine chem. industry. India). All the chemicals were used without further purification.

Preparation of local montmorillonite clay sample

Local montmorillonite clay sample collected in South Gondar Zone, Este District, Koma Kebele, Amhara region, Ethiopia was ground using a mortar and pestle and sieved through 220 mm mesh. The fine powder was dried at 110 ℃ in the oven, cooled and heated to a constant weight. In total, 20% w/v of the dried sample was dispersed in water and then 5 mL of nitric acid was added. The mixture was heated at 95 ℃ for 3 hr. The montmorillonite clay sample was filtered and washed with 50 mL of distilled water. The filtrate solid sample was dried at 80℃ for 2 hr in the oven (Du Laing *et al*., 2003).

Synthesis of nano composite

A silver nanoparticles montmorillonite clay nanocomposite was prepared using a simple chemical reduction method. Briefly, 2 g of purified local montmorillonite clay

was dispersed in 50 mL of distilled water and added 6 mL silver precursor, 0.06 $AgNO_3$ solution slowly under stirring condition. This mixture was constantly stirred for 3 hrs at 25 ℃ and heated at 80 ℃ for 30 min. Sodium citrate 3 mL of 1% was added to it and stirred vigorously for another 30 min at the same temperature to complete the reduction. The color of the mixture changed from muddy to grayish brown, which confirmed the reduction of Ag^+ to Ag-NPs. The nanocomposite material was filtered and washed repeatedly with 60 mL of distilled water to remove any physically adsorbed silver ions and calcinated at 80 ℃ for 4 hrs.

Characterization of the synthesized nanocomposite

The silver nanocomposite solution samples and MT clay were subjected to a uv-vis spectrometer between 200 and 800 nm. The reduction of silver ions and formation of silver nanoparticles due to the presence of MT clay as a support and tri sodium citrate as a reducing agent was assessed by measuring the uv-vis spectrum of the reaction medium. Fourier transform infrared (FT-IR) spectra study was used to identify the presence of MT clay and functional groups responsible for the reduction of Ag^+ ions in synthesized silver nanoparticles. The FT-IR spectra were measured by Perkin Elmer spectrometer having a resolution of 1 cm^{-1} in the wavelength range 400 - 4000 cm^{-1}. The phase purity and crystal structure was determined through XRD analysis with an X-ray source of a CuKa radiation (wavelength of 0.15406 nm) in the 2θ range of 10-60. The crystal size of the produced nanomaterials was estimated by using Debye-Scherrer formula (Ambalagi *et al*., 2016). All electrochemical experiments were performed using CHI electrochemical work station (CHI 760E) connected to a computer. A conventional three-electrode system consisting of bare and modified carbon paste electrode as working electrode, a Ag/AgCl electrode (filled with 3 M KCl) as a reference electrode and a platinum coil was employed as an auxiliary electrode.

Preparation of solution and real sample

Phosphate buffer solution (PBS), 0.1 M, a supporting electrolyte was prepared by mixing 72.2 mL of KH_2PO_4 and 27.8 mL of K_2HPO_4 solution, and diluted to 1000 mL with distilled water. A standard stock solution of arsenic (III), 300 µg/mL was prepared by transferring 30 mL standard arsenic (III) solution (1000 µg/mL) in to 100 mL volumetric flask and diluted to the mark with distilled water. The working solutions of various concentrations were prepared from the stock solution by serial dilution with 0.1M PBS.

Real sample was collected from around Kebele 7 in Bahir Dar city, Ethiopia from sewage water. The water sampled and immediately introduced into polyethylene bottles (250 mL). In total, 100 mL of water was measured and poured in to the

volumetric flask (150 mL) and added 10 mL of concentrated HNO_3; heated at 95 ℃ in hot plate. 10 mL of digested water sample was used for electrochemical measurements by diluting with 0.1 M PBS up to the mark of volumetric flask (50 mL) to determine the arsenic content.

Preparation and characterization of electrode

Graphite powder, 2 g and 1 mL of paraffin oil (in a ratio of 70:30% w/w) were mixed together in a mortar and pestle to get the bar carbon paste electrode. The modified carbon paste electrodes were prepared by mixing of Ag/MT clay composite, graphite powder and paraffin oil in the appropriate proportion.

The cyclic Voltammogram (CV) of the bare CPE and CPE/Ag/MT clay modified electrodes was evaluated using 10 mM $K_3[FeCN_6]$ in 0.1 M KCl at different scan rates (10 to 100 mV s^{-1}). CV in the presence and absence of As(III) on the bare and modified CPE were characterized in the potential range of -0.9 to 1.2 V in 0.1 M PBS (pH 7.0) at various scan rates (20 to 300 mV $s^{-1)}$. Electrochemical impedance spectroscopy experiments were performed by applying ac amplitude of 10 mV in the frequency range of 0.01 to 10, 000 Hz. Differential pulse voltammetry (DPV) oxidative current measurement was also used for characterization. A scan increment of 4 mV, pulse amplitude of 25 mV, pulse width of 80 ms, pulse period of 50 ms were the parameters selected for the differential pulse voltammetry.

RESULTS AND DISCUSSION

Uv-visible spectra analysis

Figure 1 shows the uv-vis spectra for the $AgNO_3$ solution, MT clay and the silver /MT nanocomposites recorded in the range of 300- 700 nm. No peaks were observed for both the precursor solution (curve A) and MT clay (curve B) while at the expected wave length rang of silver nanoparticles well-shaped peak centered at about 415 nm (curve C) appeared for the silver nanoparticles (Xu *et al*., 2008). This absorption peak appeared at the characteristics wave length of 415 nm could be ascribed to the so called surface Plasmon resonance of silver which is due to resonance of valence electrons of atomic silver between the conduction and valance bonds.

FTIR spectra analysis

FTIR measurements were carried out to identify various functional groups in the MT clay samples as well as in the formed Ag/MT-NCs (Figure 2). Abroad peak at 3432

cm^{-1} was the characteristics of the O-H stretching of the Al-OH, Al-Mg-O, and Fe-Mg-OH, Fe$_2$-OH as well as the OH groups of water in the clay structures. The peak observed at 1621 cm^{-1} can be assigned for H-OH bending. The peak observed at 1030 cm^{-1} was assigned for Si-O stretching, 791 cm^{-1} for (Al, Mg) - OH vibration modes, 677 cm^{-1} for Al- OH bending of MT clay structures, characteristics of MT clay minerals (Alemdar *et al.*, 2005).
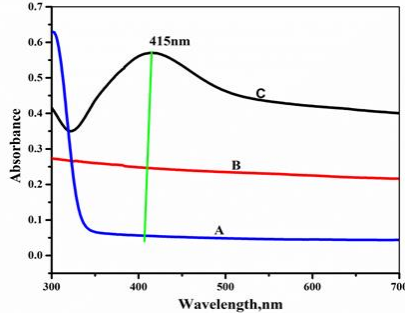
Figure 1. Uv-visible spectrum of AgNO$_3$ (curve A), MT clay (curve B), Ag-MT clay NCs (curve C).

Furthermore, the FTIR spectra of Ag-NPs showed an absorption band at 1364 cm^{-1} corresponding to the NO$_3$ stretching, which is due to the residue of silver nitrate. Besides, peak at 538 cm^{-1} and 467 cm^{-1} are most probably due to the existence of Ag-O or pure Ag-NPs (Dasaradhudu and Srinivasan, 2020). In addition, these results confirmed that with increase the amount of Ag- NPs in the Ag/MT NCs due to the existence of van der Waals interactions between the oxygen groups of MT and Ag-NPs, peak areas shifted to low wave numbers and the intensity of the peaks appearing increased. As shown in Figure 2, changes in the intensity of the spectra of Ag-MT NCs were less compared with MT clay.
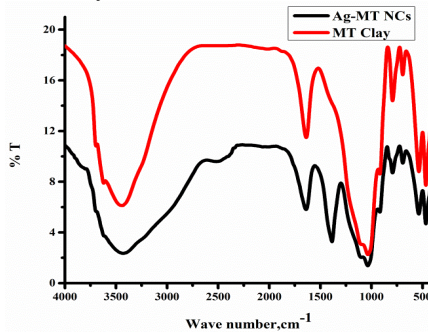
Figure 2. FTIR spectrums of MT Clay and Ag-MT NCs

The shift of the peaks at 3442 to 3433 cm^{-1} in the Ag-MT spectrum can be associated to the existence of van der Waals interactions between the hydroxyl groups of the MT layers and the partial positive charge on the surface of Ag-NPs.

XRD analysis

The XRD pattern of MT and Ag-MT NCs are shown in (Figure 3). The diffraction peaks at scattering angles (2θ): 19.8°, 21.01°, 24.26°, 27.72°, and 50.27° corresponds to the reflection from (111), (220), (311), (400), and (331) crystallographic planes of the face centered silver crystals (Prasad *et al.*, 2006). The crystalline size of nanoparticles calculated by Debye-Scherrer formula and based on the highest diffraction peak (assigned to 400 crystal plane). The 2θ value with maximum intensity of the peak for the nano composite was found to be 27.72° which corresponds to the crystal size D = 4.963 nm.

$$D = \frac{0.9\,\lambda}{\beta\cos\theta} \tag{1}$$

Where D is the crystallite size, λ is the wavelength of the X-ray = 0.15406 nm for Cu target Kα radiation, β is the peak width of half-maximum (FWHM) of an XRD (0.102114 radian), and θ is the Bragg diffraction angle (13.86). The most intense peak (400) in the XRD patterns was used to calculate the crystalline size (D). So, the crystal sizes of the silver nano particle obtained from the XRD method was 4.963 nm.
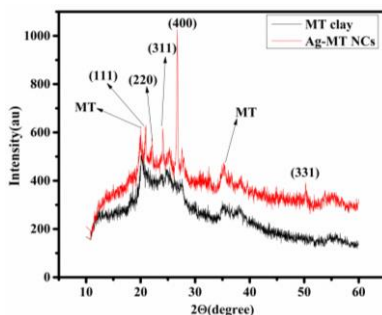
Figure 3. XRD patterns of MT and Ag-MT NCs

Electrochemistry characterization study

The Ag-MT NCs modified carbon paste electrode was characterized by cyclic voltammetry using [Fe (CN)$_6$]$^{3-/4-}$ as a probe. Figure 4 shows cyclic voltammetric response of the bare CPE (Figure 4A), and the Ag-MT NCs/CPE (Figure 4B) in 10 mM of [Fe (CN) 6]$^{3-/4-}$ containing 0.1 M KCl. A pair of reversible peaks appearing at both electrodes is attributed to a one-electron electrochemical process of [Fe (CN)$_6$]$^{3-/4-}$. The peak current response is also significantly increased at the Ag-MT NCs/CPE which could be most probably due to enhanced electrode effective surface area

and/or improved conductivity of the Ag-MT NCs modifier. The observed electrocatalytic effect of the modified CPE towards [Fe(CN)6]$^{3-/4-}$ manifested by peak potential shift and peak current enhancement is clear confirmation for the successful modification of carbon paste electrode by Ag-MT NCs.
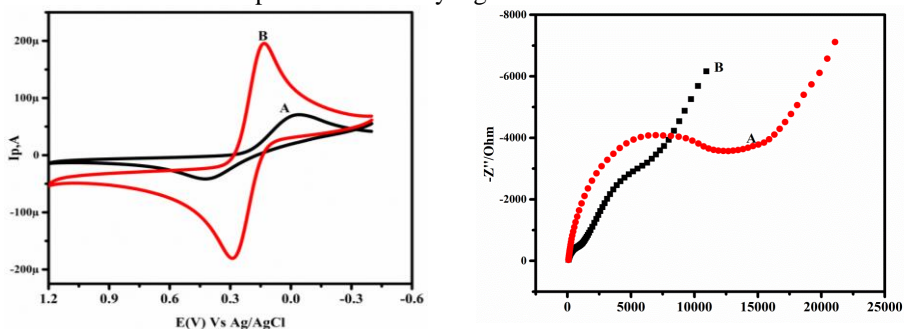
Figure 4. CVs of (A) bare CPE (B) Ag-MT NCs/CPE in 10 mM of [Fe(CN)6]3-/4- containing 0.1 M KCl. Scan rate 100 mV s^{-1} and Nyquist plots of (A) bare CPE and (B)Ag-MT NCs/CPE in 10 mM of [Fe(CN)6]$^{3-/4-}$+ 0.1 M KCl at frequency: 0.01-100,000 Hz, potential: 0.31 V, and amplitude 0.01 V.

Electrochemical impedance spectroscopy, which is a promising technique to understand the electrochemical property of the electrode surface and interface between the surface of modified electrode and electrolyte, was also used to characterize the Ag-MT NCs/CPE modified carbon paste electrode. Figure 4 shows EIS spectra of bare CPE (Figure 4A) and Ag-MT NCs/CPE (Figure 4B) in 10 mM of [Fe (CN) 6]3-/4- in 0.1 M KCl. As can be seen from the figure, significant decrease in the diameter of the semi-circle region of the Nyquist plot at Ag-MT NCs/CPE than the bare CPE indicates dramatic improvement of the conductivity of the surface leading to fast electron transfer conducting pathway between the probe and the electrode substrate.

To examine whether the fabricated Ag-MT NCs/CPE could improve the surface area and hence the conductivity of the sensor, the electroactive surface area (A) of the bare CPE and Ag-MT NCs/CPE was evaluated from the cyclic voltammograms of 10.0 mM [Fe(CN)$_6$]$^{3-/4-}$ which was recorded at varied scan rates (Figure 5). As shown in Figure 5A and B peak current of the bare, and Ag-MT NCs/CPE were proportional to the square root of the scan rates. For [Fe (CN) $_6$]$^{3,/4}$, with a number of electron n = 1 and a diffusion coefficient of D = 7.6 x 10$^{'6}$ cm s$^{'1}$, the electroactive surface area was calculated from the plot of anodic peak current versus square root of scan rate using the Randles-Sevcik formula, as 0.00358 cm^2 and 0.00588 cm^2 of the bare and Ag-MT NCs modified CPE respectively. Thus, the electroactive surface area, which measures the efficiency of the exposed surface to the catalytic reaction of Ag-MT NCs modified CPE, was increased by about 1.64 fold compared to the bare

CPE, which provided an evidence for the superior conductivity of Ag-MT NCs/CPE as expected.
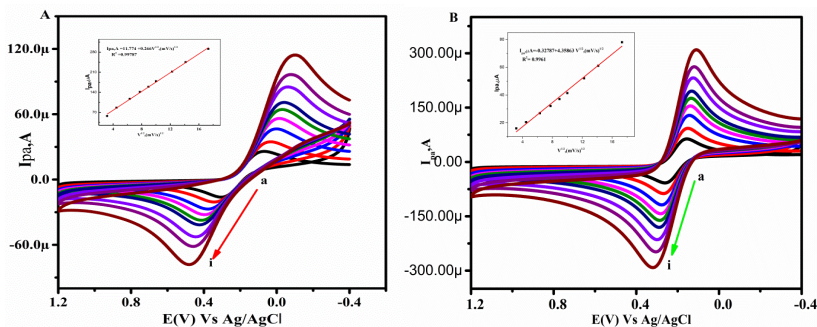
Figure 5. CVs of (A) bare (B) Ag-MT NCs/CPE in 10 mM of $[Fe(CN)6]^{3-/4-}$ + 0.1 M KCl at various scan rates (a-i : 10, 20, 40, 60, 80 , 100, 150, 200, and 300 mV s^{-1} respectively) , and inset: plot of anodic peak current versus square root of scan rate.

Electrochemical behavior of Arsenic (III)

Arsenic (III) electrochemical deposition and oxidation on Ag-MT NCs/CPE was conducted using cyclic voltammetry. As(III) concentration of 100 μg/mL deposition and oxidation on CPE was assessed in 0.1 M PBS(pH 7) and 100 mV s^{-1} scan rate. As seen in Figure 6, an anodic peak current was appeared around 0.158 V with anodic peak current of 5.57 μA on bare CPE, and increased to 123.57μA on the Ag-MT NCs/CPE. The increasing of anodic peak current intensity in the case of the modified electrode is attributed to the enhanced catalytic property of Ag-nanoparticles. It was also observed that the modified CPE provided enhanced peak intensity due to the relatively large surface area to volume ratio of Ag-MT NCs composite enabling the surface of the electrode to adsorb more As (III). In Ag-MT NCs/CPE, there are two corresponding cathodic peaks at potential of -0.149 V and current of 20.92 μA; potential -0.415 V and current of 69.89 μA for the second peak are attributed to As (III) and Ag (I) reduction, respectively. The reverse scan demonstrating that the oxidation processes of As follows an irreversible reaction. The oxidation of As at modified CPE with a dramatic increase of anodic peak current at Ag-MT NCs/CPE could be due to electrocatalytic and large electro-active surface area of the Ag-MT NCs/CPE.

The effect of scan rate on the oxidation process of As in 0.1 M PBS was studied using cyclic voltammograms on Ag-MT NCs/CPE. Figure 7A depicts recorded Voltammogram at various potential scan rates (υ = 20 to 300 mV s^{-1}). It can be noted from the voltammograms curve that, with an increase in the scan rate, there is no significant peak potential shifts. On the other hand, the oxidation current for As

increased with the scan rates. Linear relation was obtained from the plot of peak current (I_{pa}) *vs.* scan rate (υ) (Figure7B) with a regression equation I_{pa} (μA) = 83.39 +0.396υ (mV s^{-1}) (R^2 = 0.97628). This result confirms that As oxidation is an adsorption control process.
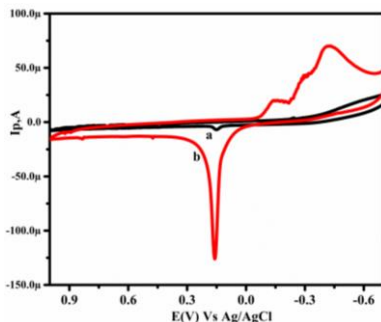
Figure 6. CVs of bare CPE (curve a) and Ag-MT NCs/CPE (curve b) of 100 μg/mL As (III) in 0.1 M PBS of pH 7.0 at scan rate of 100 mV s^{-1}.

Effect of pH

The voltammetric behavior of heavy metal ions is strongly influenced by the pH of the supporting electrolyte and thus it was essential to select a suitable pH value. The effect of pH value on the voltammetric response for 100 μg/mL of As (III) at Ag-MT NCs/CPE modified carbon paste electrode was investigated in 0.1 M PBS in the pH range of 6.0 to 8.0 using cyclic voltammetry. As shown in Figure 8A, it was noted that the anodic peak current response and the anodic peak potential value of As (III) was significantly changed with increasing pH from 6.0 to 8.0, which shows that the electrochemical reaction of As (III) is pH dependent. As it can be seen from Figure 8B, the anodic peak current increased with pH from 6.0 to 7.0 after that, it decreased as the pH reached 8. This might be due to the fact that at low pH values (< 6) As (III) exists in the neutral form (H3AsO3) that restricts its availability for adsorption. However, as the pH increased up to 7, As (III) ionized to its anionic form as H2AsO3- thus facilitating its accumulation on the surface of the Ag-MT NCs/CPE sensor. It is clearly seen from Figure 9B-a, that the anodic peak response was decreased as the pH of the solution was raised above 7. This might be due to the increased number of OH- ions that restricted the availability of H2AsO3- anions. Thus, pH 7.0 is the optimum solution pH for the analysis.

Effect of Ag-MT NCs loading

The Ag-MT NCs loading effect on the peak current response of the CPE/Ag-MT NCs for the studied metals was checked. Five carbon paste electrodes with various proportion of Ag-MT NCs modifier (3, 5, 10, 15, and 20%) were prepared. Figure 9

presents the cyclic voltammograms mixture of As (III) 100 μg/mL at carbon paste electrode loaded with various amounts of Ag-MT NCs. As indicated in the figure, the electrode modified with 10% of Ag-MT NCs revealed the most intensive anodic peaks for As (III). Thus, carbon paste electrode prepared by mixing 60% of graphite powder, 30% of paraffin oil, and 10% of Ag-MT NCs was used for further experiments.
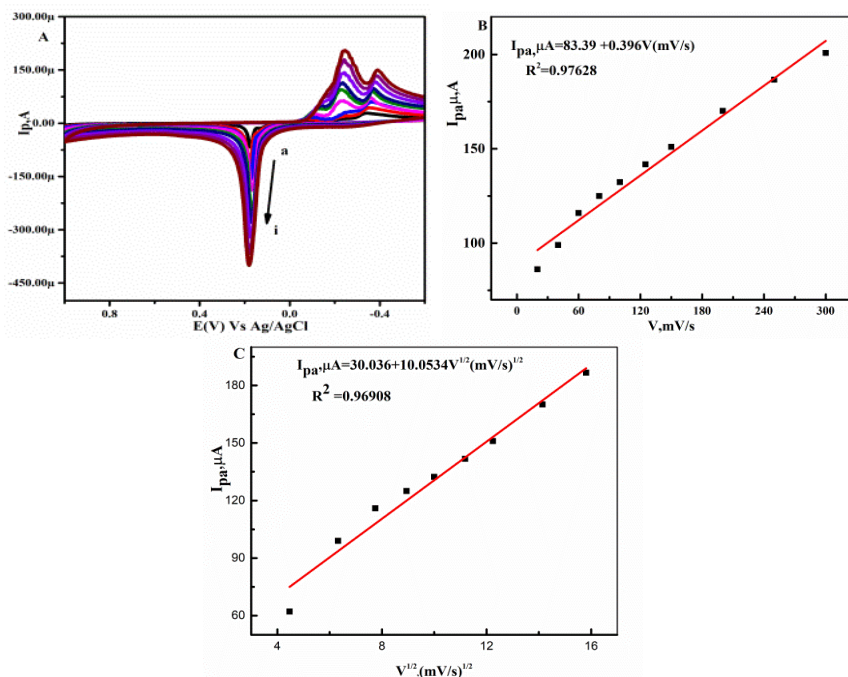
Figure 7. (A) CVs of 100 μg/mL As (III) in 0.1 M PBS of pH 5.5 at Ag-MT NCs/CPE at various scan rates (a-l:20, 40, 60, 80, 100, 150, 200, 250, and 300 mV s^{-1}, respectively). And (B) and (C) plot of anodic peak current versus scan rate and square root of scan rate respectively.

Deposition potential (E_{dep}) and Deposition time (t_{dep})

The deposition potential that gives the maximum anodic current response was optimized by varying the potential from -0.5 to -0.1 V keeping the deposition time at 60 s. It was recorded that the anodic peak current for As (III) increased from E_{dep} of -0.5 to -0.3 V as a result of more favorable alignment of As(III) ions at the Ag-MT NCs/CPE and then decreased at deposition potentials beyond -0.3 V due to the consequence of the desorption of As(III) ions from Ag-MT NCs/CPE.

Thus, E_{dep} of -0.3 V was chosen for further analysis. Likewise the optimum accumulation time was determined by fixing accumulation potential at -0.3 V. DPASVs of As(III) 100 µg/mL in *pH* 7.0 of 0.1M PBS at E_{dep} of -0.3V and various deposition times from (10 - 60 s) were measured. It was observed that, the anodic peak current response of the Ag-MT NCs/CPE for the 100 µg/mL As (III) increased from 10 to 60 s and then leveled off beyond 60 s as result of the adsorption of the As(III) ions on the Ag-MT NCs/CPE attine a saturation level and the limiting values of the deposition of As(III) ions on the Ag-MT NCs/CPE at higher deposition time. Thus t_{dep} of 60 s was chosen as the optimum deposition time.
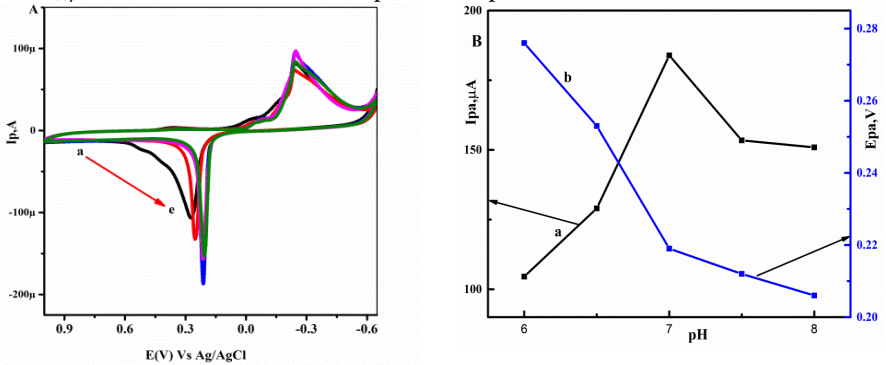
Figure 8. (A) CVs of 100 µg/mL As(III) in PBS of different pH values (a-e: 6.0, 6.5, 7.0, 7.5, and 8.0 respectively), (B) Plot of oxidative (a) peak current and (b) peak potential versus pH for 100 µg/mL As(III) at Ag-MT NCs/CPE. Scan rate: 100 mV s^{-1}.
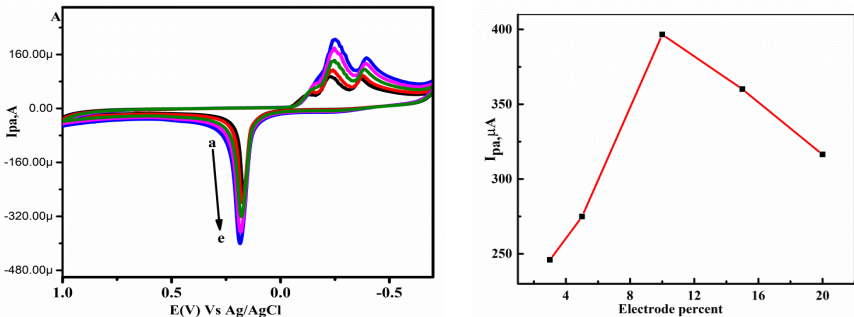
Figure 9. CVs of 100 µg/mL As(III) in 0.1 M PBS of pH 7.0 at Ag-MT NCs/CPE at various % of Ag-MT NCs (a-e: 3, 5, 10, 15, 20 %, respectively).and plot of anodic peak current versus electrode present . Scan rate: 100 mV s^{-1}.

Performance of Ag-MT NCs /CPE sensor for the determination of As (III)

To investigate the electroanalytical performance of Ag-MT NCs modified carbon paste electrode, DPASV was employed under optimal deposition potential and deposition time. DPASV oxidative peak current response of Ag-MT NCs/CPE was linearly increased with As(III) concentration in the range of 10 - 300 µg/mL (Figure 10) with a linear regression equation of Ipa (µA) = 5.985 + 0.02953 [As(III)] µg/mL and correlation coefficient, R^2 = 0.9905.
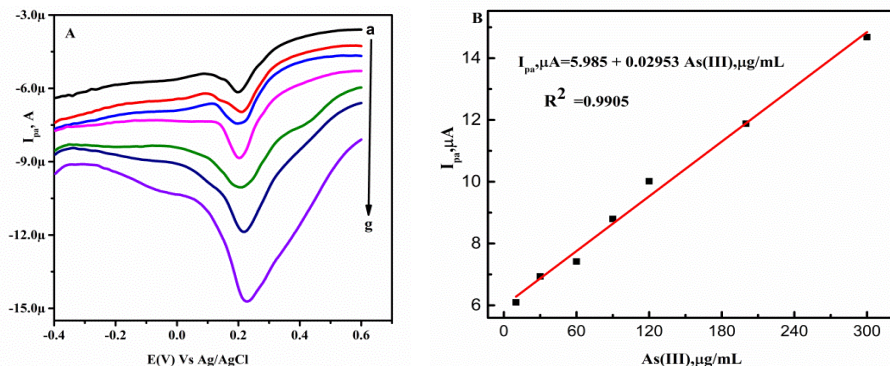
Figure 10. Corrected for blank DPVs of Ag MT NCs/CPE in pH 7.0 of 0.1M PBS containing various concentrations of As (III) (a-g: 10, 30, 60, 90, 120,200 and 300 µg/mL respectively) at deposition potential, and deposition time of -0.3 V, 60 s, respectively. And: plot of oxidative peak current versus concentration of As (III).

The sensor exhibited good sensitivity 0.02953 µA/µg/mL and limit of detection (LoD = 3 s/m) and limit of quantification (LoQ = 10 s/m); where s is blank standard deviation for *n* = 5 and *m* is the slope of the calibration graph were calculated to be 38.2 and 127.3 µg/mL, respectively. The low associated RSD values (below 5% for n=5) showed the accuracy and precision of electrode modifier. The performance of Ag-MT NCs /CPE sensor with other reported modified electrodes for the detection of As (III) are summarized in the Table 1.

Method validation

In order to see the validity of the Ag-MT NCs/CPE electrode using a chosen method, the analysis was performed for sewage water samples collected from Bahir Dar city, Ethiopia. The sample was diluted with 0.1 M PBS of pH 7.0 (1:5 ratio) and tested directly for arsenic sensing, and the actual detected amount of As(III) in the real water sample as calculated from the calibration regression equation was 498.17 µg/mL. Hence, the detection results with the proposed sensor were exhibited appreciable accuracy and precise values.

In addition, the accuracy of the method was evaluated using recovery result of spiked standards of the studied metals in the sewage water samples. 15 mL of unspiked sample and the same volume of sample spiked with 60 and 120 µg/mL of As (III) in 0.1M PBS (pH 7.0) were prepared for the recovery analysis. The percent of recovery of the added standard As (III) in the real water sample was 93.22% and 101.69% (Table 2), validating the method for determination of As (III).

Table 1. Comparison of the performance of Ag-MT NCs /CPE sensor with other reported modified electrodes for the detection of As (III)

Modified electrode	Detection method	Linear range (µg/L)	LOD(µg/L)	Reference
Au-coated BDD	DPASV	0.1-40	0.05	(Song and Swain, 2007)
IrO$_2$/GCE	DPASV	0-80	7.7	(Mafakheri *et al*., 2011)
Au-CRVfilm GCE	DPASV	300-3000	15	(Karthika *et al*., 2019)
AgNPs/Au electrode	DPASV	3.75-14.98	10.3	(Sonkoue *et al*., 2018)
AgNPs/CT-GCE	DPASV	10-100	1.2	(Prakash *et al*., 2012)
Ag-MT NCs/CPE	DPASV	10-300	4.06	This work

Table 2. Percent recovery of spiked standard As (III) solutions from real water samples

Sample	As(III) before spiked(µg/mL	As(III) added(µg/mL)	Detected As(III)after spiked(µg/mL)	Expected As(III), µg/Ml	Recovery
Real	498.17	60	554.1	558.17	93.22%
water	498.17	120	620.2	618.17	101.69%

CONCLUSION

Cyclic voltammetric and electrochemical impedance spectroscopic results fabricated Ag-MT NCs/CPE using [Fe(CN)6] $^{3-/4-}$ as a probe confirmed modification of the electrode surface by an electroactive Ag-MT NCs, which increased the electrode surface conductivity and effective surface area. Cyclic voltammetry was employed for the study of the electrochemical behavior of As (III) at the surface of the modified electrode. An irreversible anodic peak appeared at Ag-MT NCs/CPE in compression to the bare electrode the height was large, due to enhanced surface area. A good regression coefficient (R^2) for the dependence of peak current on the scan rate than on the square roots of the scan rate indicated that the oxidation reaction of As (III) at Ag-MT NCs/CPE was predominantly an adsorption-controlled. Under optimized conditions, the sensor exhibited a linear range of 10 - 300 µg/mL, low detection values of 38.2 µg/mL and quantification limit value of 127.3 µg/mL and excellent spike analysis (93.22 and 101.69%) validated the applicability of the developed method for determination of As (III) in sewage water samples.

Disclosure statement
No potential conflict of interest was reported by the author(s).

REFERENCES

Alemdar, A., Güngör, N., Ece, O and Atici, O. (2005). The rheological properties and characterization of bentonite dispersions in the presence of non-ionic polymer PEG. *Journal of Materials Science* **40**(1): 171−177.

Ambalagi, S.M., Inamadar, H.K and Sannakki, B. (2016). Mechanism of DC conductivity measurement of zinc oxide doped polyaniline nanocomposites. *Materials Today: Proceedings* **3**(10): 3945−3950.

Beyersmann, D and Hartwig, A. (2008). Carcinogenic metal compounds: recent insight into molecular and cellular mechanisms. *Archives of toxicology* **82**(8): 493−512.

Bradl, H. (2006). Adsorption of heavy metal ions on clays. *Encyclopedia of Surface & Colloid Science* **471**: 483.

Das, G., Kalita, R.D., Gogoi, P., Buragohain, A.K and Karak, N. (2014). Antibacterial activities of copper nanoparticle-decorated organically modified montmorillonite/epoxy nanocomposites. Applied Clay Science **90**: 18−26.

Dasaradhudu, Y and Srinivasan, M.A. (2020). Synthesis and characterization of silver nano particles using co-precipitation method. *Materials Today: Proceedings* **33**: 720−723.

Davies, G.-L., McCarthy, J. E., Rakovich, A and Gun'ko, Y.K. (2012). Towards white luminophores: developing luminescent silica on the nanoscale. *Journal of Materials Chemistry* **22**(15): 7358−7365.

Dharmalingam, P., Palani, G., Apsari, R., Kannan, K., Lakkaboyana, S.K., Venkateswarlu, K., Kumar, V and Ali, Y (2022). Synthesis of metal oxides/sulfides-based nanocomposites and their environmental applications: A review. *Materials Today Sustainability*: 100232.

Du Laing, G., Tack, F.M and Verloo, M.G. (2003). Performance of selected destruction methods for the determination of heavy metals in reed plants (Phragmites australis). *Analytica Chimica Acta* **497**(1-2): 191−198.

Duffus, J.H. (2002). " Heavy metals" a meaningless term? (IUPAC Technical Report). *Pure and Applied Chemistry* **74**(5): 793−807.

Haneef, F and B. Akıntuğ, B. (2016). Quantitative assessment of heavy metals in coal-fired power plant's waste water. *International Journal of Science and Technology* **2**(1): 135−149.

He, Z.L., Yang, X.E and Stoffella, P.J. (2005). Trace elements in agroecosystems and impacts on the environment. *Journal of Trace elements in Medicine and Biology* **19**(2-3): 125−140.

Karthika, A., Selvarajan, S., Karuppasamy, P., Suganthi, A and Rajarajan, M. (2019). A novel highly efficient and accurate electrochemical detection of poisonous inorganic Arsenic (III) ions in water and human blood serum samples based on SrTiO3/β-cyclodextrin composite. *Journal of Physics and Chemistry of Solids* **127**: 11−18.

Luong, J.H., Lam, E and Male, K.B. (2014). Recent advances in electrochemical detection of arsenic in drinking and ground waters. *Analytical Methods* **6**(16): 6157−6169.

Mafakheri, E., Salimi, A., Hallaj, R., Ramazani, A and Kashi, M.A. (2011). Synthesis of Iridium Oxide Nanotubes by Electrodeposition into Polycarbonate Template: Fabrication of Chromium (III) and Arsenic (III) Electrochemical Sensor. *Electroanalysis* **10**(23): 2429−2437.

Manivannan, S and Ramaraj, R. (2009). Core-shell Au/Ag nanoparticles embedded in silicate sol-gel network for sensor application towards hydrogen peroxide. *Journal of Chemical Sciences* **121**(5): 735.

Martínez-Acuña, M.I., Mercado-Reyes, M., Alegría-Torres, J.A and Mejía-Saavedra, J.J. (2016). Preliminary human health risk assessment of arsenic and fluoride in tap water from Zacatecas, México. *Environmental monitoring assessment* **188**(8): 1−13.

Prakash, S., Chakrabarty, T., Singh, A.K and Shahi, V.K. (2012). Silver nanoparticles built-in chitosan modified glassy carbon electrode for anodic stripping analysis of As (III) and its removal from water. *Electrochimica Acta* **72**: 157−164.

Prasad, V., D'Souza, C., Yadav, D., Shaikh, A and Vigneshwaran, N. (2006). Spectroscopic characterization of zinc oxide nanorods synthesized by solid-state reaction. *Spectrochimica Acta Part A: Molecular and Biomolecular Spectroscopy* **65**(1): 173−178.

Premkumar, J and Ramaraj, R. (1997). Electrocatalytic reduction of dioxygen at platinum particles deposited on Nafion-and clay-coated electrodes. *Journal of Solid State Electrochemistry* **1**(2): 172−179.

Ramaraj, R. (2006). Nanostructured metal particlemodified electrodes for electrocatalytic and sensor applications. *Journal of Chemical Sciences* **118**(6): 593−600.

Rastogi, P.K., Ganesan, V and Krishnamoorthi, S. (2014). A promising electrochemical sensing platform based on a silver nanoparticles decorated copolymer for sensitive nitrite determination. *Journal of Materials Chemistry A* **2**(4): 933−943.

Rossini, P.D.O., Laza, A., Azeredo, N.F., Goncalves, J.M., Felix, F.S., Araki, K and Angnes, L. (2020). Ni-based double hydroxides as electrocatalysts in chemical sensors: A review. *TrAC Trends in Analytical Chemistry* **126**: 115859.

Sitko, R., Janik, P., Zawisza, B., Talik, E., Margui, E and Queralt, I. (2015). Green approach for ultratrace determination of divalent metal ions and arsenic species using total-reflection X-ray fluorescence spectrometry and mercapto-modified graphene oxide nanosheets as a novel adsorbent. *Analytical chemistry* **87**(6): 3535−3542.

Song, Y and Swain, G.M. (2007). Total inorganic arsenic detection in real water samples using anodic stripping voltammetry and a gold-coated diamond thin-film electrode. *Analytica Chimica Acta* **593**(1): 7−12.

Sonkoue, B.M., Tchekwagep, P.M.S., Nanseu-Njiki, C.P and Ngameni, E. (2018). Electrochemical determination of arsenic using silver nanoparticles. *Electroanalysis* **30**(11): 2738−2743.

Xu, G.-n., Qiao, X.-l., Qiu, X.-l and Chen, J.-g. (2008). Preparation and characterization of stable monodisperse silver nanoparticles via photoreduction. *Colloids and Surfaces A: Physicochemical and Engineering Aspects* **320**(1-3): 222−226.